Original Article

MOLECULAR METABOLISM

T1R2 receptor-mediated glucose sensing in the upper intestine potentiates glucose absorption through activation of local regulatory pathways

Kathleen Smith [1,5], Elnaz Karimian Azari [1,5], Traci E. LaMoia [1], Tania Hussain [1], Veronika Vargova [2], Katalin Karolyi [1], Paula P. Veldhuis [3], Juan Pablo Arnoletti [3], Sebastian G. de la Fuente [3], Richard E. Pratley [2], Timothy F. Osborne [1], George A. Kyriazis [1,2,4,*]

ABSTRACT

Objective: Beyond the taste buds, sweet taste receptors (STRs; T1R2/T1R3) are also expressed on enteroendocrine cells, where they regulate gut peptide secretion but their regulatory function within the intestine is largely unknown.
Methods: Using T1R2-knock out (KO) mice we evaluated the role of STRs in the regulation of glucose absorption *in vivo* and in intact intestinal preparations *ex vivo*.
Results: STR signaling enhances the rate of intestinal glucose absorption specifically in response to the ingestion of a glucose-rich meal. These effects were mediated specifically by the regulation of GLUT2 transporter trafficking to the apical membrane of enterocytes. GLUT2 translocation and glucose transport was dependent and specific to glucagon-like peptide 2 (GLP-2) secretion and subsequent intestinal neuronal activation. Finally, high-sucrose feeding in wild-type mice induced rapid downregulation of STRs in the gut, leading to reduced glucose absorption.
Conclusions: Our studies demonstrate that STRs have evolved to modulate glucose absorption via the regulation of its transport and to prevent the development of exacerbated hyperglycemia due to the ingestion of high levels of sugars.

Keywords Glucose homeostasis; Sweet taste receptors; GLP-2; GLUT2; T1R2

1. INTRODUCTION

Glucose handling in response to a meal requires the integration of several diverse mechanisms that originate from a variety of organs aiming to coordinate delivery to peripheral cells. Although organs such as the liver, pancreas, and skeletal muscle are central to the regulation of glucose homeostasis, ingested glucose first encounters the gastrointestinal (GI) tract, which determines its systemic rate of appearance. Yet, there is still limited understanding of how the plethora of GI tract tissues and pathways coordinate the regulation of post-ingested glucose metabolism [1].
For instance, enteroendocrine L-cells integrate signals from glucose and other nutrients to release glucagon-like peptides-1 and -2 (GLP-1 and GLP-2), peptide YY (PYY), and oxyntomodulin which exert pleiotropic effects locally and in remote target organs [2]. Among these, GLP-1 is the most studied due to its potent incretin effects and other glucoregulatory roles [3], which led to widely used GLP-1-based antidiabetic therapies [4]. However, these enteroendocrine peptides are coordinately released in response to specific stimuli, raising the possibility that the mixture of L-cell secreted hormones might play complementary roles to regulate acute nutrient availability. For example, GLP-1 and GLP-2 are derived from proteolytic cleavage of the proglucagon protein and are co-released in 1:1 ratio [5]; however, unlike the well-defined role of GLP-1, the contribution of GLP-2 in postprandial glucose regulation is elusive [6].
Peptide secretion from enteroendocrine cells is regulated by apical chemoreceptors that are responsive to free fatty acids (GRP40, GRP120, CD36), amino acids (umami; T1R1/T1R3 heterodimer), and simple sugars (sweet taste receptors; STRs; T1R2/T1R3 heterodimer) [7] indicating that receptor-mediated nutrient sensing in the gut is pivotal to the regulation of ingested nutrient availability. For instance, activation of STRs can stimulate peptide release from mouse and

[1]Center for Metabolic Origins of Disease, Sanford Burnham Prebys Medical Discovery Institute, Orlando, FL, USA [2]Translational Research Institute for Metabolism and Diabetes, Florida Hospital, Orlando, FL, USA [3]Institute for Surgical Advancement, Florida Hospital, Orlando, FL, USA [4]Department of Biological Chemistry and Pharmacology, College of Medicine, The Ohio State University, Columbus, OH, USA

[5] Kathleen Smith and Elnaz Karimian Azari contributed equally to this work.

*Corresponding author. Department of Biological Chemistry and Pharmacology, College of Medicine, The Ohio State University, 460 W 12th Ave, Columbus, OH 43210, USA. E-mail: kyriazis.2@osu.edu (G.A. Kyriazis).

Abbreviations: STRs, sweet taste receptors; KO, knock out; GI, gastrointestinal; GLP-1 and GLP-2, glucagon-like peptides-1 and -2; PYY, peptide YY; IG.GTT, intragastric glucose tolerance test; IP, intraperitoneal; 3-OMG, 3-O-methylglucose; HPV, hepatic portal vein; TER, tissue trans-epithelial resistance; I_{sc}, short-circuit current; P_{app}, apparent permeability coefficient; EEC, enteroendocrine cells; Gcg, pro-glucagon; TTX, tetrodotoxin; HSD, high sucrose diet; WAT, white adipose tissue

Received May 18, 2018 • Revision received August 9, 2018 • Accepted August 22, 2018 • Available online 27 August 2018

https://doi.org/10.1016/j.molmet.2018.08.009

human intestinal L-cells [8–10], but the context and physiological relevance of these gut-related pathways *in vivo* is still unclear. Notably, however, the expression of intestinal STR in individuals with type 2 diabetes negatively correlates with luminal and plasma glucose levels [11,12], suggesting the potential involvement of STRs in the development of metabolic disease that may be mediated by critical gut-related mechanisms.

Using mice with genetic ablation of the T1R2 receptor (T1R2-knock out; KO) to eliminate STR signaling [13], we demonstrate a comprehensive integrated model by which STR-mediated glucose sensing in the upper intestine is required for the potentiation of glucose absorption. This regulatory pathway is dependent on L-cell-derived GLP-2 secretion that mediates the apical translocation of the GLUT2 glucose transporter in enterocytes through local neuronal activation. In addition, we also show that in WT mice, intestinal STRs are rapidly downregulated by acute consumption of excess dietary sugars, causing reduced peptide secretion and glucose absorption, mirroring our findings with T1R2-KO mice. These findings reveal a mechanism where regulation of STR signaling in L-cells controls glucose absorption in enterocytes to limit postprandial hyperglycemia in response to high consumption of dietary sugars.

2. MATERIALS & METHODS

2.1. Animals and diets

All animal experimental procedures were approved by the Institutional Animal Care and Use Committee (IACUC) of the Sanford Burnham Prebys Medical Discovery Institute (SBP). Whole body T1R2-deficient mice (T1R2-KO; gift by Dr. Zuker) or double STRs deletion (T1R2/R3-KO; generated in our lab) were used with age matched, gender matched, in-house bred WT mice (C57Bl\6J) as controls. All mice are back-crossed on the C57Bl\6J strain for at least 10 generations. Animal studies were performed on 8- to 12-week old male and female mice maintained on regular chow diet (Harlan-Teklad 2016). For experiments involving special diets, 8-week old mice were acclimatized on control diet (60% Corn starch D12328, Research diets) for one week. Then, mice were placed on a high sucrose diet (60% sucrose; D12329, Research diets) or continued the control diet for either one additional day (i.e. a single overnight feeding cycle) or for 7 days.

2.2. Glucose administration *in vivo*

For intragastric (IG) and intraperitoneal (IP) glucose tolerance test (GTT), fasted mice received 1 g/kg body weight (BW) of glucose. Blood glucose was sampled from the tail and analyzed with an AlphaTRAK blood glucose monitoring meter (North Chicago, IL). Glucose tolerance curves X time are shown in absolute values. Rate of plasma glucose excursion was calculated using glycemic slope between 0 and 15 min. Area under curve (AUC) was calculated using the trapezoid method adjusted to individual baselines. For frequent sampling IG.GTT, catheters were surgically implanted into the left common carotid artery and right jugular vein as described [14], except that anesthesia was induced (2%) and maintained (1–2%) with isoflurane. The arterial catheter was used to obtain blood samples in conscious, unrestrained mice. After a 5-day recovery, mice were fasted for 5 hours (h) and then received an IG.GTT. Blood samples were obtained at 0, 3, 6, 9, 12, 15, and 30 min. For the assessment of glucose absorption *in vivo*, mice were gavaged with D-[^{13}C]-glucose (0.5 g/kg) and 3-O-methylglucose (3-OMG; 0.5 g/kg) or 3-OMG (1 g/kg) alone and plasma excursion was monitored at 0, 5, 15, and 30 min by tail vein blood collection. For *in vivo* [Gly^2]-GLP-2 (teduglutide; Caslo Laboratory, Denmark) experiments, mice received an IP injection of either PBS (vehicle) or 0.9 μg/g BW teduglutide immediately followed by either an IG.GTT or IP.GTT. The stock solution was prepared in Dimethylformamide (DMF) and then diluted in PBS to achieve the final concentrations. Tail vein blood was collected at 0, 15, 30, and 45 min and blood glucose was monitored by AlphaTRAK blood glucose monitoring meter (North Chicago, IL). For the assessment of GLUT2 translocation from the basolateral membrane to the apical membrane, 5 h-fasted mice received an IG.GTT (4 g/kg) including 0.4% trypan blue or PBS (vehicle) with 0.4% trypan blue. After 15 min, mice were euthanized and the proximal intestine was collected up to the section where the dye was visible to determine the distance the glucose solution had traveled. The length of the entire intestine was measured and used to determine luminal glucose transit as % of total intestine. Luminal glucose transit rate (cm/min) was separately calculated for IG.GTT including 1 g/kg or 4 g/kg.

2.3. Plasma hormones

For GLP-1 measurements, mice were fasted for 5 h and blood samples were collected from tail veins at 0, 5, 15, and 30 min following an IG.GTT (1 g/kg). For GLP-2 measurements, mice were fasted for 5 h and hepatic portal vein (HPV) samples were collected 15 min following an IG.GTT (1 g/kg) or PBS (vehicle).

The collected blood was immediately transferred to EDTA-coated microcentrifuge tubes (Sarstedt AG & Co.) containing 0.6TIU aprotinin (Phoenix Pharmaceuticals Inc.), and 10 μl of DPPIV inhibitor (EMD Millipore) per 1 mL of blood. Plasma was obtained by centrifugation at 1500 × g for 15 min at 4 °C and stored at −80 °C until measurement of total GLP-1 (Crystal Chem, Elk Grove Village, IL, USA, cat # 81508), or total GLP-2 (MyBioSource, San Diego, CA, USA). Plasma insulin was assessed with an ultra-sensitive ELISA kit (Crystal Chem, Inc, Downer's Grove, IL, USA). Plasma corticosterone was measured in mice that were fed *ad libitum* (0 h), or fasted for 5 h, or 16 h. Blood was collected via tail vein (25 μL) in heparin coated tubes and plasma was isolated by centrifugation at 1500 × g at 4 °C for 15 min and stored at −80 °C until the measurement of corticosterone levels (Enzo Life Sciences, Farmingdale, NY).

2.4. Gastric emptying

The acetaminophen absorption test was used to assess the rate of gastric emptying [15]. Mice fasted for 5 h were gavaged with the mixture of glucose (1 g/kg) and acetaminophen (0.1 g/kg). Tail-vein blood (50 μL) was collected in heparin coated tubes at 0, 15, 30, 45, and 60 min after the mixture administration. Plasma was separated as above and stored at −80 °C until measurement of acetaminophen levels by the Exploratory Pharmacology Core by LC-MS/MS.

2.5. Fecal processing

Fresh feces (100–150 mg) were collected in the morning, snap frozen in liquid N_2, and stored at −80 °C until processing. Fecal extracts were processed for LC-MS/MS analysis by mixing 50 mg of feces with 500 μL of phosphate buffer (0.1 M K_2HPO_4/NaH_2PO_4 = 4/1, pH 7.4) containing 30% D_2O, 0.002% (w/v) of sodium 3-(trimethylsilyl) propionate-2,2,3,3-d4 (TSP), 0.03% of Na_3N (w/v). After vortex mixing, the samples were subjected to a freeze-thaw cycle in liquid nitrogen 3 times and subsequently homogenized with a polytron homogenizer at max speed for 90 s, followed by centrifugation at 10,000 × g for 10 min at 4 °C. Supernatants were collected and the remaining pellet was further extracted once, as described above. Supernatants from the two runs of extraction were combined and centrifuged at 10,000 × g for 10 min at 4 °C. The final supernatant was given to the Exploratory Pharmacology Core for analysis.

2.6. LC-MS/MS

Plasma (20 μL) containing [U-^{13}C6]-glucose, acetaminophen, or 3-OMG was added to 180 μL of acetonitrile with 1 μg/mL of indomethacin and vortexed for 5 min at room temperature. Samples were then centrifuged at 3700 rpm at 4 °C for 20 min. The supernatant was transferred to a 96-well plate and dried under gentle N_2 stream at 40 °C at 20 cc/min. 100 μL of MPA:MPB (80%:20%) was added to each sample, mixed well, and centrifuged for 10 min. The resulting extract (100 μL) was injected on a Thermo HPLC system equipped with PAL CTC plate sampler (96-well plate), Dionex Ultimate 3000 binary pump (flow rate at 0.25 mL/min), Dionex Ultimate 3000 thermostatted column compartment (temperature at 40 °C), Thermo Endura Mass Spectrometer (ESI source), using Phenomenex Luna® NH_2 (5 μm, 2 × 100 mm, 100 Å) column under isocratic conditions of MeOH aq (40 μM CsOAc, 0.1% formic acid) starting at 80% during 0.75 min. Under gradient condition of 80—100% MeOH aq (40 μM CsOAc, 0.1% formic acid) over 0.5 min, finishing at 100% MeOH aq (40 μM CsOAc, 0.1% formic acid) over 2 min, returning to 80% MeOH aq over 0.5 min and kept at 80% MeOH aq for another 1 min to re-equilibrate. For quantification, 3-OMG, acetaminophen, and [U-^{13}C6]-glucose were diluted in DMSO, then spiked into plasma to generate calibration curves. For fecal glucose, glucose was spiked into the buffer to generate a calibration curve. The peak area was measured and analyte amounts were calculated referring to analyte calibration curves. Analyte levels were adjusted with IS concentration for extraction efficiency. Peak height measurements were conducted referring to values obtained for standards of known concentrations.

2.7. Energy balance

Indirect calorimetry was assessed using the Comprehensive Lab Animal Monitoring System (CLAMS; Columbus Instruments) of the Cardiometabolic Phenotyping Core, SBP. Mice were placed in individual metabolic cages for at least 24 h to acclimate. Next, measurements were taken every 15 min over a 48 h period. Oxygen consumption (VO_2) and carbon dioxide production (VCO_2) were measured to obtain estimates of energy expenditure and substrate utilization. Energy expenditure was calculated using the following equation:$(3.815 + 1.232*(VCO_2/VO_2))*VO_2$ [16]. Food intake was measured using a precision scale. Water intake was measured using a volumetric drinking dispenser. Ambulatory activity was estimated by the number of infrared beam breaks along the x-axis of the metabolic cage. Average energy expenditure, energy intake and water intake was calculated as the average of two dark cycles.

For experiments involving special diets, food intake was assessed manually. Mice were individually housed and allowed to acclimatize for 3 days. A pre-determined amount (g) of the diet (i.e. CON and HSD) was provided to each mouse and food intake was measured every 24 h for 5 consecutive days. The amount of food weighed was subtracted from the previous day to determine grams of food consumed the past 24 h period.

2.8. Ussing chamber

Ad libitum mice euthanized with CO_2 and the entire small intestine was rapidly removed and flushed with ice-cold Krebs—Ringer Bicarbonate (KRB) solution. All small intestinal sections including duodenum, jejunum, and ileum were removed, cut along the mesenteric border, and pinned onto Ussing chamber sliders with a 0.25 cm^2 open surface area (P2404, Physiologic Instruments, San Diego, CA, USA). The sliders with sections were inserted into Ussing chamber at 37 °C in the presence of 3 mL oxygenated (95% O_2 and 5% CO_2) KRB buffer (NaCl 115 mM, K_2HPO_4 2.4 mM, KH_2PO_4 0.4 mM, $CaCl_2$ 1.2 mM, $MgCl_2$ 1.2 mM, $NaHCO_3$ 25 mM with pH 7.4). Sections were equilibrated for 20—30 min in KRB buffer containing 10 mM D-mannitol in the mucosal chamber and an equal concentration of D-glucose in the serosal chamber to maintain osmotic balance. Subsequently, the solutions were replaced with different glucose/3-OMG concentrations in the mucosal chamber and the respective concentration of mannitol in the serosal chamber, as described below. To control for tissue viability and integrity, tissue trans-epithelial resistance (TER) values were monitored constantly throughout the experiments. Tissues with reduced TER values more than 15—20% from the values at the end of the equilibration period were excluded.

Short-circuit current (I_{sc}): To determine SGLT1 mediated D-glucose transport, changes in I_{sc} were monitored in response to glucose. The resulting I_{sc} was blocked by addition of the selective SGLT1 inhibitor, phlorizin (0.5 mM; 4627, Tocris, United Kingdom), to the mucosal chamber. The absolute difference in I_{sc} values from baseline to maximal/minimal changes following D-glucose or phlorizin are expressed as ΔI_{sc}.

Isotopic flux studies: All D-glucose and 3-OMG flux studies were performed from mucosal-to-serosal direction using the mid-distal jejunum and under steady-state conditions with 30 min of equilibration. A) Unlabeled D-glucose (5—30 mM) with [^{3}H]-D-glucose (1.0—2.5 μCi) was added to the mucosal chamber and flux to the serosal chamber was examined with or without phlorizin (0.5 mM) or phloretin (0.5 mM), added at 60 min. B) Unlabeled 3-OMG (10—30 mM) with [^{14}C]-3-OMG (1.0—1.5 μCi) was added to the mucosal chamber and flux to the serosal chamber was examined with or without phloretin (0.5 mM) or tetrodotoxin (2 μM), added at 60 min. Teduglutide (200 nM) was added to the serosal chamber of seromuscular stripped intestine at time 0. Samples (10 μL) were collected from the serosal chamber in 30 min intervals for 2 h and radioactivity was determined by scintillation counting machine (Perkin—Elmer). Any background or non-specific binding was subtracted by the measurements. The unidirectional apparent permeability coefficient (P_{app}; cm/min) was calculated from the following equation [17]: $P_{app} = (dQ/dt)*V/(C_0*A)$, where dQ/dt is the rate of appearance of the compound (nmol/mL) from the mucosal to serosal chamber over time (min), V is the volume (mL) of the chamber, C_0 is the initial total donor concentration (nmol/mL) of the compound ($t = 0$), A is the functional surface area (cm^2). The unidirectional flux (J; nmol/min/cm^2) was determined by the following equation: $J = (dQ/dt)/A$. Relative inhibition was calculated as $P_{app}[dt_{(90\text{-}120)}]/P_{app}[dt_{(30\text{-}60)}]$ for vehicle or treatment (i.e. phloretin, phlorizin, TTX) added at $t = 60$.

Flux studies in human samples: The study was approved by the Institutional Review Board (IRB) at Florida Hospital. Tissues was collected from the proximal intestine of men and women undergoing scheduled (non-emergent) gastrointestinal surgery at the Institute for Surgical Advancement, Florida Hospital. All potential subjects were recruited by Florida Hospital, interviewed prior to their participation, and excluded according to the following criteria: 1) Younger than 18 years, 2) Unable to provide written, informed consent, 3) Chronic oral or injected steroids (inhaled steroids for mild asthma are acceptable), 4) Chronic antibiotic use.

One hour prior to collection, RPMI media supplemented with glutamax was oxygenated and kept cold under sterile conditions. After resection, the intestine was flushed with ice cold DPBS to wash off contents, cut into two 2 × 2 cm squares and placed in the media. The tissue was then transported from Florida Hospital to SBP within 30 min under continuous oxygenation. The adipose and muscle layers were carefully removed and the mucosa was mounted in the Ussing chamber with an exposed tissue area of 0.25 cm^2. Sections were equilibrated as above. Unlabeled 3-OMG (30 mM) and [^{14}C]-3-OMG (1 μCi) were added to the

mucosal chamber. Lactisole (2 mM) was also added to the mucosal chamber at timepoint 0 and samples were collected every 30 min for 2 h. Integrity of the tissue was determined at the end of the experiment by assessing the tissue's response to the addition of carbachol (200 nM) at the serosal chamber. Samples that did not respond were excluded from the analysis.

2.9. NCI-H716 L-cells

Human enteroendocrine NCI-H716 cells (ATCC, CCL-251, Manassas, VA, USA) were obtained from the American Type Culture Collection. The cell-line was validated through the expression of the proglucagon gene (gcg) and GLP-1 secretion. The cells were grown in suspension culture RPMI 1640 medium supplemented with 10% FBS, 100 IU/mL penicillin, and 100 μg/mL streptomycin. Fresh media was added to the cells twice a week. For GLP-1 secretion experiments, NCI-H716 cells were plated at a density of 1×10^6 in 6-well cell culture plates pre-coated with Matrigel™ basement membrane matrix (BD Biosciences, San Jose, CA) diluted (1:100) in DMEM high glucose (4 g/L) serum free medium. Medium was changed every day until the day of the experiment. Two days after differentiation, the growth media was removed, and the cells were washed twice with PBS. Glucose concentrations of 5 mM or 25 mM were prepared in PBS buffer supplemented with 1 mM $CaCl_2$, pH adjusted to 7.2, pre-warmed to 37 °C, and pre-incubated on the cells (3 mL/well) for 12 h at 37 °C in a humidified incubator at 5% CO_2. After 12 h, cells were washed twice with PBS and incubated for 1 h in PBS with 5 mM or 25 mM glucose supplemented with 1 mM $CaCl_2$. DPP-IV inhibitor (EMD Millipore, Burlington, MA) was added to the solutions (20 μL/mL). After 1 h, the plate was immediately placed on ice to stop further secretion. The medium was collected and centrifuged at 4 °C for 10 min at 3,000 rpm to remove cell debris. Supernatant was collected and stored at −80 °C until GLP-1 determination. Cells were homogenized with 0.1 M NaOH and protein concentration per well was measured by BCA assay (Thermo Fisher Scientific). Total GLP-1 was assayed using an ELISA (Millipore) and normalized to protein content. For RNA isolation, cells were incubated with 5 mM or 25 mM glucose in PBS supplemented with 1 mM $CaCl_2$ for 12 h. After 12 h, the cells were washed with PBS, trypsinized with 0.25% trypsin for 5 min, collected, and spun down at 3000 rpm for 5 min, trypsin removed and washed with PBS to remove the trypsin. Cells were spun a second time, supernatant removed, and the pellets frozen at −80 °C until RNA could be isolated by Direct-zol RNA isolation kit (Zymo Research, Irvine, CA).

2.10. Intestinal morphology

Intestinal sections were collected, flushed with ice-cold PBS, cut open, and rolled along the longitudinal axis to prepare intestinal Swiss-rolls, as previously described [18]. Sections were fixed in 4% paraformaldehyde (PFA) solution at 4 °C, paraffin embedded, and 5 μm sections stained with hematoxylin and eosin. Villus height, mucosal surface area, and crypt depth were assessed as described [19] on Swiss-roll intestinal cross-sections using the *ImageJ* software (NIH). An average value from minimum of 200 villi and crypts was calculated for each intestinal segment per mouse.

2.11. Immunofluorescence

For double label immunostaining, mice were fasted for 5 h to eliminate luminal contents and were gavaged either with distilled water or 4 g/kg BW of glucose. Subsets of animals received, at the time of glucose gavage, an IP injection of either saline (Vehicle), teduglutide (0.9 mg/kg BW; Teduglutide), or Exendin-4 (3 pg/kg). After 15 min, jejunal sections were flushed with ice-cold PBS containing phenylmethane sulfonyl fluoride (PMSF, ThermoFisher scientific, 36978), and intestinal Swiss-rolls were prepared. GLUT2 colocalization with sucrase isomaltase, a specific marker for the brush-border membrane [20], was assessed. The collected intestinal Swiss-rolls were fixed overnight in 4% PFA and embedded in paraffin. Sections of 10 μm in thickness were deparaffinized and then unmasked in citric buffer (pH 6.0) for 15 min in a microwave oven. After being cooled to room temperature for 20 min and washed in PBS—0.1% Tween-20 (PBS-T), nonspecific binding sites were blocked with 1%BSA in PBS-T for 1 h at room temperature. Slides were incubated with mixtures of rabbit anti-GLUT2 antibody (1:200, sc-9117, Santa Cruz Biotechnology) and goat anti-sucrase isomaltase antibody (1:100, sc-27603, Santa Cruz Biotechnology) diluted in blocking buffer overnight at 4 °C. Slides were then washed twice with PBS-T and incubated with Alexa Fluor 647- and 488-conjugated secondary antibodies (donkey anti-rabbit and anti-goat, ThermoFisher scientific) for 1 h at room temperature. Samples were washed in PBS twice and then counterstained with Hoescht 33258 dye (1:5000, ThermoFisher scientific) for 5 min. Finally, slides were washed in PBS and mounted in ProLong Gold (ThermoFisher scientific). Subsequently images were acquired using a Nikon A1R VAAS inverted confocal microscope. Quantitative colocalization analysis was performed using the Pearson's correlation coefficient (Velocity image processing, PerkinElmer) in 5—8 images for each mouse.

For single immunofluorescence staining, intestinal Swiss-rolls from mice without any treatments were used and processed. For GLP1 and chromogranin A (marker of enteroendocrine cells) antibodies, the blocking buffer solution contained 10% normal donkey serum (NDS) in PBS. Antibodies to GLP1 (sc-7782, Santa Cruz Biotechnology) and chromogranin A (sc-1488, Santa Cruz Biotechnology) were incubated with 5% NDS in PBS with dilutions of 1:100. Control slides were treated with antibody diluent in place of primary antibody followed by the secondary antibody. No positive staining was observed under these conditions.

2.12. Ex vivo glut2 apical translocation

Mice (8—10 week) were euthanized, their abdomens were opened longitudinally, and the entire small intestine was excised out. The small intestine was flushed with ice-cold L-15 media and kept in L-15 media on ice. Then, each intestine was flushed and rinsed with ice-cold KRH and was inverted and placed in either 30 mL of warmed (37 °C) glucose solution (5 mM or 50 mM) with continuous oxygenation (95% O2/5% CO2) for 10 min. Next, PMSF (0.5 mM) was added to each preparation and allowed to incubate for additional 5 min. The intestine was then removed, rinsed with ice-cold KRH with PMSF (0.5 mM), and the mucosa was scraped using a microscope slide and snap-frozen until brush border membrane vesicles were isolated.

2.13. Intestinal tissue preparation and fractionation

Mucosal Scrapings and Serosa Collection: 15—20 cm of duodenum and jejunum were excised out and flushed with ice cold PBS treated with 0.1 mM PMSF to arrest GLUT2 in the apical membrane. Next, the intestine was inverted using a Hamilton syringe so that the mucosa was facing out; then it was rinsed in ice-cold PBS with PMSF and placed onto an ice-cold glass plate. The mucosa was gently scraped from the serosal layer using an ice-cold glass slide at a 45° angle with mild pressure. Scraped tissue was transferred to aluminum foil and snap frozen in liquid N_2. The remaining serosal tissue was transferred to a 1.5 mL Eppendorf tube and snap frozen.

Nuclear Fractionation and Total Membranes: To prepare nuclear fractions, the serosa was homogenized with a dounce homogenizer in 1 mL of ice-cold homogenization buffer (20 mM Tris, HCl pH 7.4—7.6,

2 mM $MgCl_2$, 0.25 mM sucrose, 10 mM EDTA, 10 mM EGTA, 1 mM PMSF) and treated with protease and phosphatase inhibitors. The tissue was dounced 30 times and transferred to a 1.5 mL Eppendorf tube and centrifuged at 3,000 × g for 5 min. The supernatant was removed and the pellet is resuspended in 100 μL of nuclear lysis buffer (20 mM HEPES pH 7.6, 420 mM NaCl, 1.5 mM $MgCl_2$, 5.0 mM EDTA, 5.0 mM EGTA, 25% glycerol, 1 mM PMSF) treated with inhibitors. Next, samples were rotated for 1 h at 4 °C and centrifuged at 50,000 rpm at 4 °C for 20 min in an ultracentrifuge. The resulting supernatant was the nuclear fraction. The protocol above was also used to prepare total membranes from the mucosa, except the first supernatant of the initial spin was placed into 1.7 mL ultracentrifuge tubes and centrifuged for 53,000 rpm at 4 °C for 45 min. The resulting supernatant is the cytoplasmic fraction and is removed. The pellet is resuspended in 100 μL of membrane resuspension buffer (10 mM Tris HCl pH 6.8, 100 mM NaCl, 1% SDS, 1 mM EDTA, 1 mM EGTA, 1 mM PMSF) and supplemented with protease inhibitors and rotated for 1–3 h at room temperature to allow membranes to solubilize.

Brush Border Membrane Vesicles (BBMV): Snap frozen mucosal scrapings were homogenized for 3 min with a polytron in 15 mL of ice-cold homogenization buffer (300 mM mannitol, 5 mM EGTA, 12 mM Tris–HCl, pH 7.1) supplemented with protease inhibitor cocktail (Sigma, P8340) and 1 mM PMSF. Next, 20 mL of ice cold water with MgCl2 (20 mM final) was added to each sample (final vol. 35 mL) and mixed by inversion at 4 °C for 15 min for divalent cation precipitation. Samples were centrifuged at 3,000 × g at 4 °C for 15 min to separate aggregated membranes and the supernatants were carefully transferred to a new tube for a second centrifugation at 30,000 g at 4 °C for 30 min. Pellets were re-suspended in 35 mL of 150 mM mannitol, 2.5 mM EGTA, 6 mM Tris–HCl, pH 7.1. Next, MgCl2 was added (20 mM final) and mixed by inversion at 4 °C for 15 min. Next, samples were centrifuged at 3,000 × g for 15 min. The supernatant was carefully transferred to a new tube and centrifuged at 30,000 g at 4 °C for 30 min. The final BBMV pellet was re-suspended in 50 μl sterile PBS and stored at −80 °C.

2.14. Western blotting

Samples from isolated BBMVs (30 μg), serosal nuclear fractions (30 μg), or total membrane (30 μg) were separated by SDS-PAGE and blotted onto nitrocellulose membranes. After blocking non-specific sites, total membranes or BBMVs were probed for Glut2 (cat#20436-1-AP, Proteintech, Rosemont, IL), custom purified rat Glut2 raised using the first extracellular loop (AA 40–56: SHYRHVLGVPLDDRRA; 21st Century Biochemicals, Marlboro, MA, USA), PepT1 (cat# sc-20653, Santa Cruz, Dallas, TX), SGLT1 (cat# ab14686, Abcam, Cambridge, UK) or NaKATPase (cat# ab7671, Abcam). Nuclear fractions were probed with c-fos (9F6) (cat# 2250S, Cell Signaling, Danvers, MA), p-c-fos (Ser32) (cat# 5348S, Cell Signaling), and YY1 (cat# sc281, anta Cruz). Total membrane fractions were probed with T1R3 (cat# NB10098792, Novus Biologicals, Littleton, CO) and NaKATPase. All antibodies were used with the recommended dilutions and detected by enhanced chemiluminescence using Supersignal West Pico or Femto Chemiluminescent Substrate (cat# 34080, cat#37074, Thermo Scientific, Rockford, IL). Images were taken using a Kodak Image Station 4000 mm Pro and signal intensity was quantified using ImageJ software, version 1.8 (NIH).

2.15. Gene expression

Total RNA from scraped intestinal mucosa was extracted by TriZOL method per manufacturer's protocol. For NCI-H716 cells, RNA was isolated using the Direct-zol RNA isolation kit according to the manufacturer's instructions. Primer sequences: cDNA synthesis was performed using the ABI High Capacity cDNA kit with 1 μg of RNA. Real-time quantitative PCR was performed on the BioRad CFX Real-Time PCR Detection System with BioRad iQ™ Sybr® Green Supermix for the following genes: *T1r1* (forward: ACAGGTTGGTCATGGGTT, reverse: TGGCAGGTGTGAAGCTC), *T1r2* (forward: GAACTGCCCAC-CAACTACAA, reverse: CCATCGTGGACAGACATGAA), *T1r3* (forward: CCAGTGAGTCTTGGCTGACA, reverse: TTCAGTGAGGCACAGAATGC), *Sglt1* (forward: TGGAGTCTACGCAACAGCAAGGAA, reverse: AGCCCA-CAGAACAGGTCATATGCT), *Glut2* (forward: CCCTGGGTACTCTTCAC-CAA, reverse: GCCAAGTAGGATGTGCCAAT), *Glut5* (forward: AAAGACACACAGACACTCCCTGCT, reverse: TCCCTTGGTGCTCAC-CATGTAACT), *Glut7* (forward: CTACGTGGTAATCCCTGAAACC, reverse: CCGTGGCTACTTCTTTCTCTTC), *Glut9* (forward: GATGATGTCT GTCCTGGATGTAG, reverse: GAGTGATGTCGGGTGTCTTT), *Glut10* (forward: GCTTTGAATGAAGGAAGGGATTAG, reverse: CAGGGCTT-TAGGAAGTCAGTAG), *Gcg* (forward: CTGGTCAAAGGCCGAGGAAG, reverse: TGGTTGTGAATGGTGAAATACCT), *Glp2r* (forward: TCATCTCC CTCTTCTTGGCTCTTAC, reverse: TCTGACAGATATGACATCCATCCAC), human *TAS1R2* (Forward: AAAGAGCTGCCCACCAACTA, Reverse: CAGGAGGTTGAGCACAGTGA). Relative quantitation of transcript levels was analyzed using the 2-ΔCT with Ct values obtained from PCR amplification kinetics measured by the BIORAD CFX Manager 3.1 software. GAPDH RNA (*gapdh*) was used for normalization, as its intestinal expression remained unaltered independent of mouse genotype or diet.

2.16. Statistics

Results are shown as mean+/-SEM. The level of significance was set at $p < 0.05$. Statistical tests and significance were calculated as shown in figure legends.

3. RESULTS

3.1. Ablation of T1R2 sugar sensor in mice reduces glucose absorption *in vivo*

We have shown that whole-body T1R2 knockout (T1R2-KO) have similar responses to WT mice during an IP.GTT or a hyperglycemic clamp [21,22]. Because STRs are also expressed in the intestine, we subjected T1R2-KO mice to an IG.GTT to test whether this route of glucose administration would alter its plasma excursions. Unlike the IP.GTT, plasma glucose responses were reduced in T1R2-KO mice at the onset of the IG.GTT compared to WT mice (Figure 1A). Accordingly, T1R2-KO mice showed significant reduction (35%) in the rate of plasma glucose excursion (Figure 1A) immediately following the glucose gavage, suggesting altered glucose absorption. These differences were not due to intensified early phase insulin responses (Figure 1B). Similar effects were noted between WT and mice lacking both STR receptors (T1R2/R3-KO) (Supp. Figure 1A), confirming the specificity of STR signaling. No differences in the rate of plasma glucose excursion were noted between T1R2-KO and T1R2/R3-KO ($p = 0.061$). Next, we used conscious unrestrained mice in which an arterial catheter had been surgically implanted allowing frequent blood sampling. Compared to WT, T1R2-KO mice had consistently reduced plasma glucose excursions soon after the IG.GTT (Figure 1C). To exclude a role of endogenous glucose turnover, we gavaged mice with [U-^{13}C6]-glucose and monitored its plasma concentrations. Plasma [U-^{13}C6]-glucose levels were reduced in T1R2-KO mice compared to WT mice (Figure 1D), suggesting that the lower plasma glucose levels during the IG.GTT were due to reduced rate of glucose excursion. Finally, these observations in T1R2-KO mice cannot be

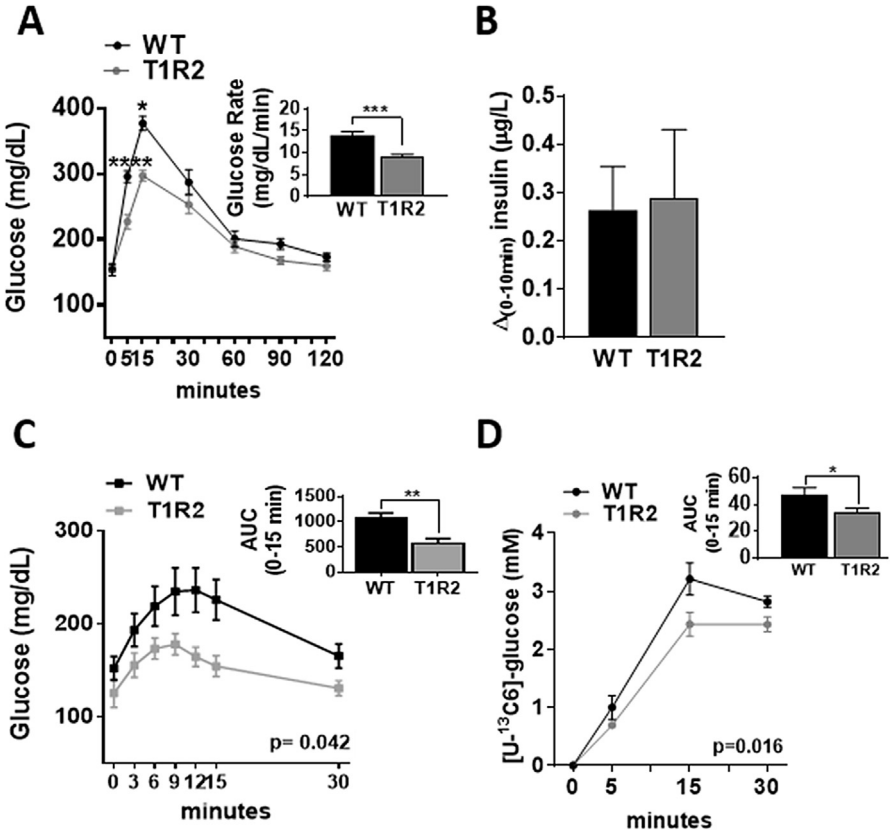

Figure 1: Plasma glucose excursions in response to a glucose gavage in WT and T1R2-KO mice. A) Plasma glucose responses (mg/dL) during an IG.GTT ($n = 10$ mice/group). Two-way ANOVA with post-hoc; *$p < 0.05$, ****$p < 0.0001$. Inset: rate of glucose excursions (mg/dL/min) at the onset of the IG.GTT. Student's t-test; ***$p < 0.001$. **B)** Plasma insulin responses (μg/L) at the onset of an IG.GTT ($n = 7–8$ mice/group). **C)** Plasma glucose responses (mg/dL) during an IG.GTT in unrestrained catheterized mice ($n = 6–7$ mice/group). Two-way ANOVA, genotype main effect; $p = 0.042$. Inset: area under curve (AUC) adjusted to individual baselines. Student's t-test; **$p < 0.01$. **D)** Plasma [U-^{13}C6]-glucose responses (mM) during an IG.GTT ($n = 8–9$ mice/group). Two-way ANOVA, genotype main effect; $p = 0.016$. Inset: calculation of AUC. Student's t-test; *$p < 0.05$.

attributed to differences in transit rate of luminal glucose (Supp. Figure 1B), glucose malabsorption (Supp. Figure 1C), or chronic disruptions in energy balance (Supp. Figure 1D).

3.2. T1R2 signaling in gut endocrine cells regulates GLUT2 translocation to the apical membrane of enterocytes in response to high luminal glucose

The SGLT1 and GLUT2 transporters control intestinal glucose absorption [23,24], so we assessed their role in the T1R2-KO intestines. We noticed a moderate reduction in the expression of *Glut2* (18%), *Glut5* (24%), and *Glut7* (30%) in the duodenum, but total protein levels of GLUT2 in the proximal intestine were similar among genotypes (Supp. Figure 2A–C). No differences in the overall expression of other sugar transporters (Supp. Figure 2C) and taste receptor genes were noted (Supp. Figure 2D). At moderate levels of luminal glucose SGLT1 is the primary glucose transporter [24], so we compared SGLT1-mediated *ex vivo* glucose transport in intestinal explants of WT and T1R2-KO mice using the Ussing chamber technique. SGLT1-mediated glucose transport, assessed by the measurement of the short circuit current (I_{sc}), peaked at mid-jejunum, but no differences between genotypes were observed in the I_{sc} (Supp. Figure 2E) or in the rate of intestinal glucose flux (Supp. Figure 2F) in the presence of 10 mM glucose. Addition of phlorizin, an SGLT1 specific inhibitor, completely and equally abolished the I_{sc} (Figure 2A) and the apparent permeability coefficient (P_{app}) of glucose in both genotypes (Figure 2B). Similar inhibitory effects of phlorizin were noted at saturated glucose concentrations (30 mM) for SGLT1 (Supp. Figure 2G). Taken together, these data suggest that the T1R2 chemoreceptor regulates glucose absorption without altering SGLT1 activity.

Next, we assessed the role GLUT2 transporter because, in response to high luminal glucose (>20 mM), GLUT2 can translocate from the basolateral to the apical membrane to enhance glucose uptake [23]. Although a glucose gavage induced an anticipated GLUT2 translocation to the apical membrane in WT intestines *in vivo*, these effects were dramatically reduced in T1R2-KO mice (Figure 2C). Similarly, GLUT2 was enriched in BBMV from WT isolated intestines incubated at high glucose, but these effects were absent in T1R2-KO intestines under the same conditions (Figure 2D). Next, we evaluated *ex vivo* glucose transport, but because elevated ambient glucose concentrations increase glucose oxidation in enterocytes [25], we used the non-metabolizable glucose analogue, ^{14}C-3-O-methyglucose (^{14}C-3-OMG). Additionally, 3-OMG and glucose are equally sweet [26]. Strikingly, the rate of flux was considerably lower (48%) in T1R2-KO intestines in response to the addition of high 3-OMG concentrations (30 mM), but not at low concentrations (10 mM), at which its transport is independent of GLUT2 (Figure 2E). The genotype effects were not due to differences in tissue resistance (Supp. Figure 2H). STRs in the GI tract may regulate ingested glucose in humans [27], so we used fresh

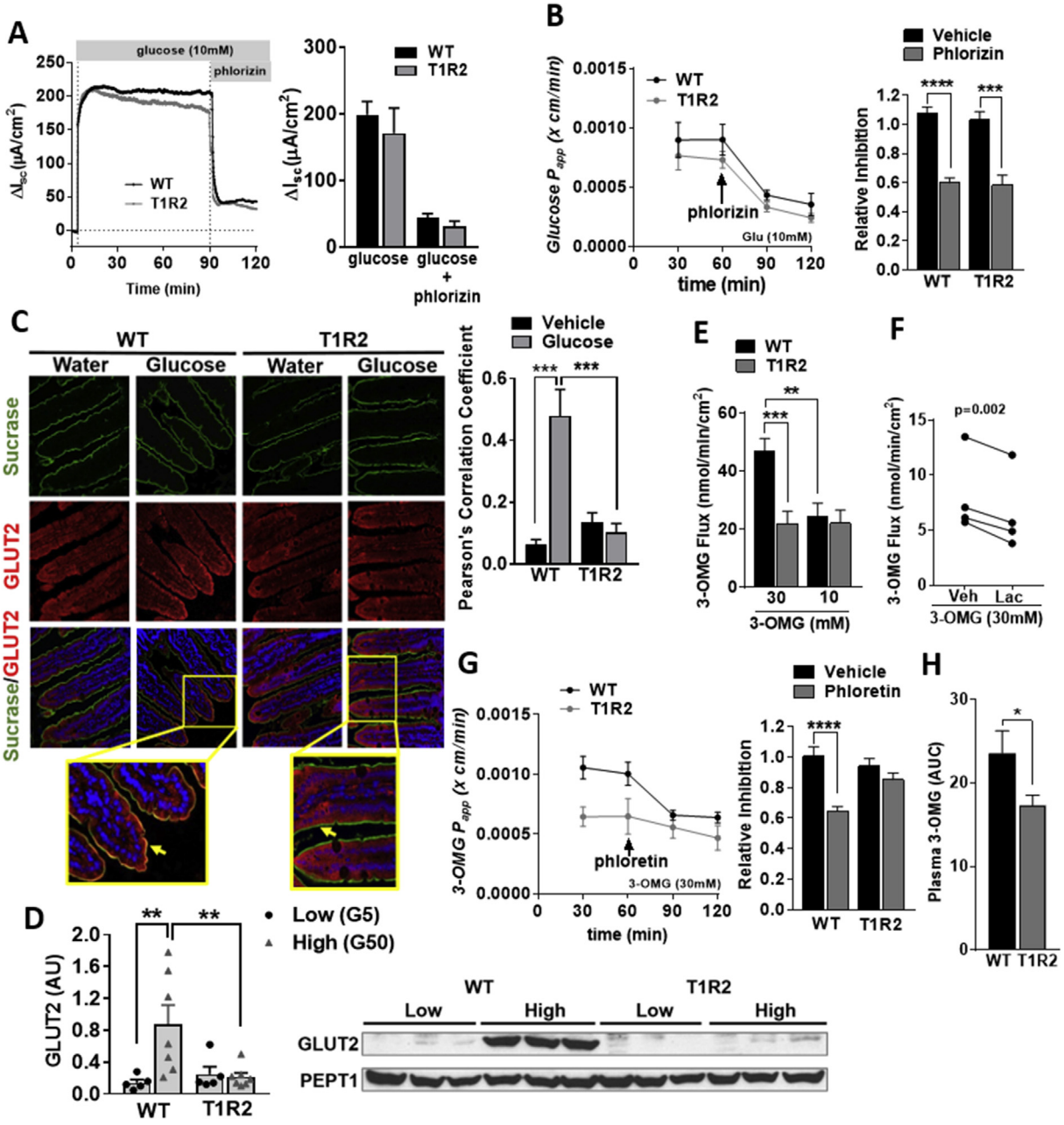

Figure 2: Contribution of SGLT1 and GLUT2 transporters in the regulation of glucose absorption in WT and T1R2-KO intestines. **A)** SGLT1-mediated glucose transport in isolated intestines assessed by short-circuit current (ΔI_{sc}; $\mu A/cm^2$) in the presence of 10 mM glucose followed by the addition of phlorizin. Average trace is shown (n = 7–9 mice/group). **B)** SGLT1-mediated glucose transport in isolated intestines assessed by the apparent permeability coefficient (P_{app}) in the presence of 10 mM glucose followed by the addition of phlorizin (n = 6–8 mice/group). Student's t-test (one-tailed); ***$p < 0.001$, ****$p < 0.0001$. **C)** Immunofluorescence of GLUT2 translocation to the brush border membrane (BBM) of intestinal mucosa *in vivo* in response to water or glucose gavage. Green: sucrase (apical membrane marker), Red = GLUT2, Blue: DAPI. Arrows show BBM. Quantification using Pearson's correlation coefficient for the co-localization of sucrase and GLUT2 (n = 4 mice/group). One-way ANOVA with post hoc; ***$p < 0.001$. **D)** Immunoblotting of GLUT2 translocation to the BBM of intestinal mucosa in isolated intestines *ex vivo* incubated at basal (Low; 5 mM) or stimulated (High; 50 mM) glucose (G). Arbitrary units (AU) of glut2 intensity adjusted for pept1, a BBM enrichment marker (n = 5-7 mice/group). One-way ANOVA with post hoc; **$p < 0.01$. **E)** Rate of 3-OMG flux (nmol/min/cm^2) in intact intestinal preparations in the presence of 10 mM and 30 mM 3-OMG (n = 6–8 mice/group). One-way ANOVA with post hoc; **$p < 0.01$; ***$p < 0.001$. **F)** Rate of 3-OMG flux (nmol/min/cm^2) in intact human intestinal explants in the presence of 30 mM 3-OMG with or without lactisole (n = 4 donors). Paired Student's t-test; $p = 0.002$. **G)** GLUT2-mediated glucose transport in isolated intestines assessed by the P_{app} in the presence of 30 mM 3-OMG followed by the addition of phloretin (n = 7–9 mice/group). Student's t-test (one-tailed); ****$p < 0.0001$. **H)** Plasma 3-OMG excursions expressed as area under curve (AUC; 0–15 min) at the onset of an oral gavage of 3-OMG (n = 7–8 mice/group). Student's t-test; *$p < 0.05$.

human surgical explants to test *ex vivo* glucose flux during pharmacological inhibition of STRs with lactisole [28]. Lactisole reduced glucose flux in human intestinal preparations, mirroring the effects of genetic ablation of STRs in mouse intestines (Figure 2F). To test GLUT2 specificity, we used the selective inhibitor phloretin which reduced relative trans-epithelial 3-OMG flux in WT intestines, but had little effect in T1R2-KO intestines where flux was already lower (Figure 2G). In contrast, phloretin had no inhibitory effect at low concentrations of glucose (Supp. Figure 2I), suggesting that the genotype effects on GLUT2 are evident only in response to high ambient concentrations of glucose or its analogue. Finally, as with isolated intestines, plasma excursion of 3-OMG was reduced in T1R2-KO mice *in vivo* following an IG. administration (Figure 2H). Taken together, our data suggest that the intestinal T1R2 chemoreceptor alters glucose absorption, at least in part, by locally modulating GLUT2 activity.

3.3. GLP-2 mediates the effects of T1R2 signaling in the regulation of GLUT2 translocation and glucose absorption

STRs are expressed in enteroendocrine L-cells but glucose transport occurs in enterocytes, so we reasoned that an endocrine/paracrine factor should likely mediate these effects. First, we measured GLP-1 during an IG.GTT and found reduced responses in T1R2-KO mice (Figure 3A), confirming previous findings using T1R3-KO and gusducin-KO mice [8,10]. GLP-1 can modulate gastric emptying [29], but plasma appearance of acetaminophen [15] were similar between genotypes in response to a glucose gavage (Figure 3B). Because GLP-2 may regulate GLUT2 trafficking [30], we measured GLP-2 in hepatic portal vein (HPV) blood, which is representative of the local gut milieu, at the onset of the gavage. Glucose induced a mild GLP-2 increase in WT mice, but not in T1R2-KO mice (Figure 3C). Glucocorticoids and insulin can also regulate GLUT2 translocation [31,32], but no differences were detected between genotypes in the plasma levels of these hormones (Supp. Figure 3A and Figure 1B). Moreover, no differences between genotypes were noted in the abundance of total enteroendocrine cells (EEC) and L-cells (Supp. Figure 3B), or in the expression of the pro-glucagon (*Gcg*) gene (Supp. Figure 3C). Taken together, these findings suggest that the reduced GLP-1 and GLP-2 responses in T1R2-KO mice were likely due to interrupted STR signaling and secretion mechanisms and not due to secondary defects in other hormones or enteroendocrine cell differentiation.

To test whether GLP-2 locally mediates the regulatory effects of T1R2 signaling on GLUT2 translocation *in vivo*, we used [Gly^2]-GLP-2 (Teduglutide), a stable synthetic GLP-2 analogue [33]. A single IP injection of teduglutide immediately prior to an IG.GTT did not alter plasma glucose excursions in WT mice, but completely restored plasma glucose excursions in T1R2-KO mice at the onset of the IG.GTT (Figure 3D). Next, we performed an IP.GTT to bypass the GI tract. IP injection of teduglutide prior to an IP injection of glucose did not alter plasma glucose responses in T1R2-KO or in WT mice (Figure 3E), suggesting the gut as the major site of GLP-2 regulation. Similar to *in vivo* responses, pre-treatment with teduglutide did not potentiate trans-epithelial 3-OMG flux in WT intestines *ex vivo*, but restored the blunted 3-OMG flux in T1R2-KO intestines (Figure 3F). These findings cannot be explained by altered expression of intestinal GLP-2 receptor (Supp. Figure 3D). Next, we tested whether activation of submucosal/myenteric neurons is required for GLP-2-induced glucose transport [34]. IG. glucose administration rapidly promoted the accumulation of the phosphorylated nuclear form of cfos (p-cfos), which is a marker of neuronal activation, in intestinal mesenchymal tissue of WT mice, but this was significantly blunted in the intestines of T1R2-KO mice (Figure 3G). In contrast, IP. teduglutide administration, that bypasses STRs, caused the accumulation of nuclear p-cfos in both WT and T1R2-KO intestines (Supp. Figure 3E). Consistent with these findings, neuronal inhibition with tetrodotoxin (TTX) reduced P_{app} of 3-OMG in WT intestines, but TTX had little effect on the already reduced 3-OMG flux in T1R2 intestines (Figure 3H). Nevertheless, when teduglutide was added along with 3-OMG to restore flux in T1R2 intestines, TTX treatment equally abolished 3-OMG flux in both genotypes (Figure 3I). Taken together, these observations suggest that at least part of the stimulatory effects of glucose and GLP-2 require enteric neuronal activation.

Then, we determined whether teduglutide rescued the T1R2-KO phenotype via GLUT2 regulation. IP injection of teduglutide alone induced the apical translocation of GLUT2 (Figure 3I) [30]. Although teduglutide followed by an IG.GTT had no additive effects on GLUT2 translocation in WT intestines compared to the IG.GTT alone, it completely restored GLUT2 translocation in T1R2-KO intestines (Figure 3I), consistent with the plasma glucose excursion data (Figure 3D). In contrast, IP injection with a GLP-1 analogue (exendin-4) alone or prior to an IG.GTT did not modulate GLUT2 translocation in WT or T1R2-KO intestines (Figure 3I) confirming GLP-2 specificity. Finally, villus height, crypt depth, total mucosal surface area, and total length of the small intestine were similar between WT and T1R2-KO mice (Supp. Figure 3F), excluding a trophic role of GLP-2 [35].

3.4. Acute feeding of a diet high in sucrose induces the downregulation of STRs in the gut leading to reduced glucose absorption

STR expression can be acutely regulated by ambient glucose [22]. Thus, we tested whether overnight feeding with high dietary simple sugars (60% sucrose) can regulate intestinal STR expression and function compared to control complex carbohydrate diet (60% corn starch). No differences in food intake were observed among diets or genotypes (Supp. Figure 4A). High sucrose diet (HSD) induced significant downregulation of mRNA expression of the *T1r2* and *T1r3* genes for WT and the *T1r3* gene for T1R2-KO mice throughout the small intestine (Figure 4A) but not in white adipose tissue (WAT), which also expresses STR [36,37] (Supp. Figure 4B). As expected, HSD feeding upregulated the fructose transporter, glut5, (Supp. Figure 4C) [38] but not the glucose transporters, *Sglt1* and *Glut2*. Because the T1R3 STR is required for the upregulation of *Sglt1* in response to chronic HSD [39], we tested whether *Sglt1* expression was unexpectedly regulated by the high-starch content of control diet. However, we found no differences in *Sglt1* expression between control and chow diet, that is low in starch (Supp. Figure 4D), confirming that overnight HSD feeding has no *bona fide* effect on glucose transporter expression.

The downregulation of STRs in the gut was accompanied by functional alterations in glucose absorption because WT mice on HSD had significantly lower glucose excursions immediately after an IG.GTT (Figure 4B) but these effects disappeared when glucose was administered via IP injection (Supp. Figure 4E), excluding differences in peripheral glucose disposal. Unlike in WT mice, diet had no effect in T1R2-KO mice (Figure 4C). Differences in plasma glucose levels in HSD fed WT mice cannot be attributed to altered insulin responses at the onset ($t = 0-5$ min) of the IG.GTT (Supp. Figure 4F), but were likely due to reduced glucose absorption assessed with an IG. [U-^{13}C6]-glucose gavage (Figure 4D). As expected, plasma [U-^{13}C6]-glucose in T1R2-KO was reduced independent of diet, suggesting a direct link between the effects of HSD and STR signaling.

HSD feeding also reduced GLP-1 responses in WT mice (Figure 4E), consistent with the reduced expression of STRs under the same conditions (Figure 4A). As expected, T1R2-KO mice had reduced GLP-1

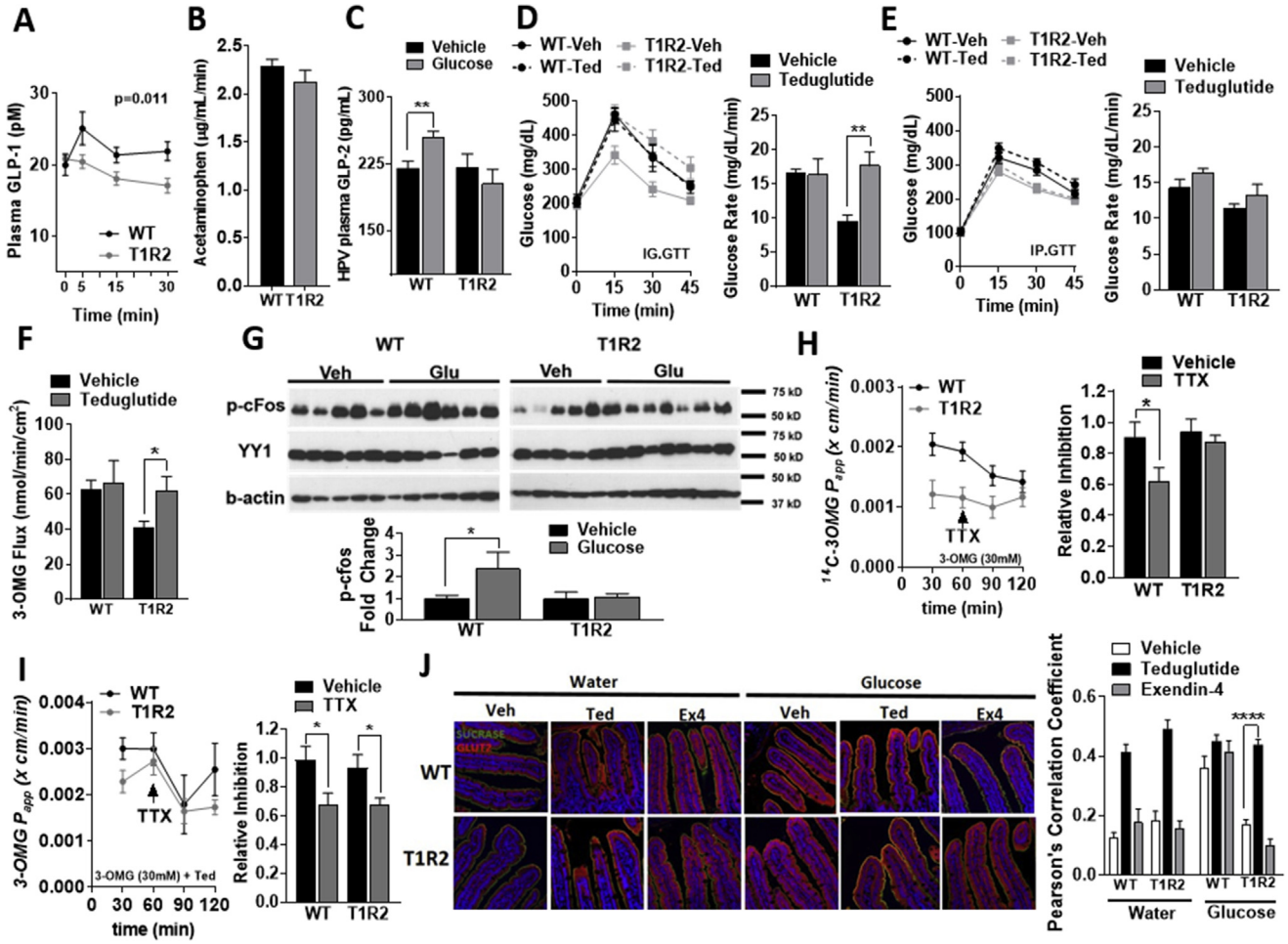

Figure 3: Contribution of GLP-2 in the regulation of GLUT2-mediated glucose absorption in WT and T1R2-KO mice. A) Plasma GLP-1 responses (pM) during an IG.GTT ($n = 14–16$ mice/group). Two-way ANOVA; time x genotype main effect, $p = 0.011$. **B)** Estimation of gastric emptying by measuring the rate of plasma acetaminophen (µg/mL/min) in response to an IG. gavage ($n = 7–8$ mice). **C)** GLP-2 responses (pg/mL) in blood collected from the hepatic portal vein 15 min after an IG. gavage of glucose or water (Vehicle) ($n = 5$ mice/group). Student's t-test (one-tailed); $^{**}p < 0.01$. **D-E)** Plasma glucose responses (mg/dL) during an IG.GTT ($n = 5–7$ mice/group) and an IP.GTT ($n = 4$ mice/group) that were preceded by a single IP. injection of teduglutide or vehicle. Rate of glucose excursions (mg/dL/min) at the onset of the GTT. Student's t-test (one-tailed); $^{**}p < 0.01$. **F)** Rate of 3-OMG flux (nmol/min/cm^2) in intact intestinal preparations in the presence of 30 mM 3-OMG with or without the addition of teduglutide ($n = 6$ mice/group). Student's t-test (one-tailed); $^{*}p < 0.05$. **G)** Phosphorylated cfos (p-cfos) in nuclear mesenchymal fractions in response to IG. Vehicle (Veh) or glucose (Glu) gavage in mice. YY1 is a nuclear marker ($n = 5–7$ mice/group). Student's t-test (one-tailed); $^{*}p < 0.05$. **H)** Apparent permeability coefficient (P_{app}) in the presence of 30 mM 3-OMG followed by the addition of tetrodotoxin (TTX) ($n = 6$ mice/group). Student's t-test (one-tailed); $^{*}p < 0.05$. **I)** P_{app} in the presence of 30 mM 3-OMG and 200 nM teduglutide (Ted) followed by the addition of TTX ($n = 6$ mice/group). Student's t-test (one-tailed); $^{*}p < 0.05$. **J)** GLUT2 translocation to the apical of intestinal mucosa. Green: sucrase (apical membrane marker), Red: GLUT2. Quantification using Pearson's correlation coefficient for the co-localization of sucrase and GLUT2 ($n = 7–8$ mice/group). One-way ANOVA with post hoc; $^{****}p < 0.0001$ (only relevant differences are shown).

responses independent of diet (Figure 4E). Next, we cultured NCI-H716 enteroendocrine L-cells at elevated glucose overnight (12 h) to simulate the effects of HSD feeding and test the association between STR expression and peptide secretion *in vitro*. Similar to *in vivo* findings, expression of STRs in NCI-H716 L-cells was acutely suppressed by elevated glucose (Figure 4F) and correlated with reduced glucose-stimulated GLP-1 secretion (Figure 4G). Taken together, these findings suggest that intestinal STRs are downregulated by HSD to modulate gut hormone responses and glucose absorption. Finally, we fed mice a HSD for 7 days and found prominent sustained reduction in STRs expression specifically at the proximal intestine, but not at the tongue (Figure 4H). HSD feeding induced glucose intolerance in both genotypes (Supp. Figure 4G), but T1R2-KO mice were protected against HSD-induced hyperglycemia (Figure 4I), suggesting that functional downregulation in STR-mediated glucose absorption may be key to prevent exacerbated hyperglycemia during periods of excess sugar consumption.

4. DISCUSSION

We have unveiled a previously underestimated gut-specific pathway in which receptor-mediated glucose sensing controls post-ingested glucose metabolism. Using both genetic and pharmacological manipulations *in vivo* and *ex vivo*, we show that glucose-dependent stimulation of intestinal T1R2/T1R3 chemosensors on L-cells enhances glucose absorption through GLP-2-mediated activation of GLUT2 transporter in enterocytes (Figure 5). In comparison to other known glucose sensing mechanisms on L-cells [24,40], the physiological significance of this pathway is emphasized when luminal glucose concentrations are high, such as during a sugar-rich meal.

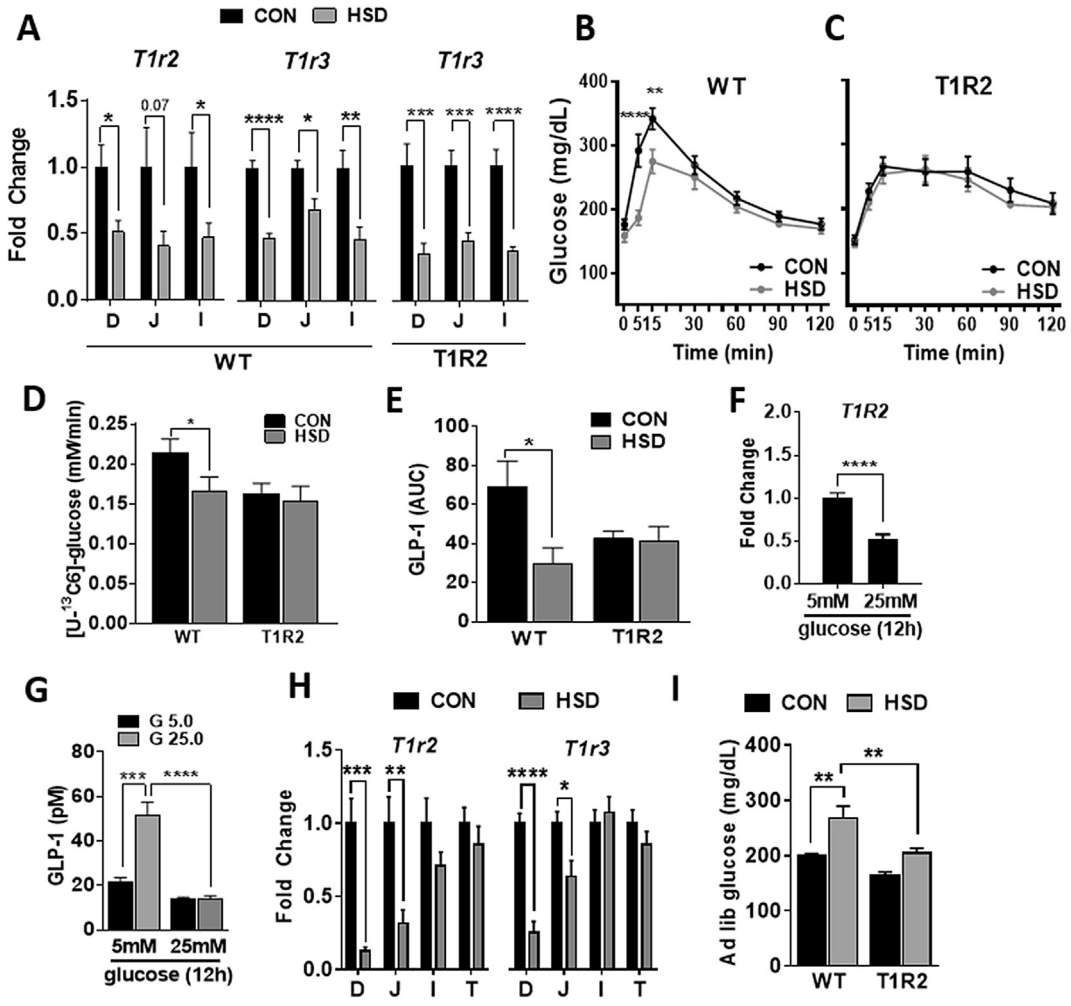

Figure 4: Effects of short-term high sucrose feeding in the regulation of intestinal STR expression and function in WT and T1R2-KO mice. A) Relative gene expression of t1r2 and t1r3 in intestinal mucosa of mice fed control (CON) diet or high-sucrose diet (HSD) overnight ($n = 11-14$ mice/group). Student's t-test; *$p < 0.05$, **$p < 0.01$, ***$p < 0.001$, ****$p < 0.0001$. D = Duodenum; J = Jejunum; I = Ileum. **B-C)** Plasma glucose responses (mg/dL) during an IG.GTT in mice fed CON or HSD overnight ($n = 6-12$ mice/group). Two-way ANOVA, post hoc; **$p < 0.01$, ****$p < 0.0001$. **D)** Rate of plasma [U-^{13}C6]-glucose appearance (mM/min) at the onset of an oral gavage in mice fed CON or HSD overnight. ($n = 7-8$ mice/group). Student's t-test; *$p < 0.05$. **E)** Plasma GLP-1 responses (area under the curve for $t = 0-30$ min) during an IG.GTT in mice fed CON or HSD ($n = 8-10$ mice/group). Student's t-test; *$p < 0.05$. **F)** Relative gene expression of t1r2 in differentiated NCI-H716 L-cells cultured in low (5 mM) or high (25 mM) glucose for 12 h ($n = 6$). Student's t-test, ****$p < 0.0001$. **G)** Static GLP-1 secretion (pM) at basal (5.0 mM) and stimulated (25.0 mM) glucose (G) concentrations in NCI-H716 L-cells cultured either at low (5 mM) or high (25 mM) glucose for 12 h ($n = 4$). One-way ANOVA with post hoc; ***$p < 0.001$, ****$p < 0.0001$. **H)** Relative gene expression of t1r2 and t1r3 in intestinal mucosa of WT mice fed CON or HSD for 7 days ($n = 8$ mice/group). Student's t-test; *$p < 0.05$, **$p < 0.01$, ***$p < 0.001$, ****$p < 0.0001$. T = Tongue. **I)** *Ad libitum* plasma glucose (mg/dL) levels in mice fed CON or HSD for 7 days. ($n = 6$ mice/group). One-way ANOVA with post hoc; **$p < 0.01$.

This is an adaptive pathway, which can be rapidly downregulated in response to the consumption of high levels of sugars, likely to prevent exacerbated post-prandial hyperglycemia. Towards this end, our data also demonstrate that T1R2-mediated co-secretion of GLP-1 and GLP-2 coordinates the fate of postprandial glucose and, for the first time, provides a plausible physiologic rationale for the coordinated secretion of GLP-1 and GLP-2 in regulating glucose metabolism.

Among other mechanisms, glucose-induced activation of the T1R2/T1R3 chemosensors on L-cells stimulates the secretion of peptides. Thus, T1R2-KO mice have impaired glucose-stimulated GLP-1 and GLP-2 secretion, consistent with previous reports using T1R3-KO or gustducin-KO mice [8,10]. Accordingly, IG infusion of glucose plus lactisole in humans reduced GLP-1 compared to glucose alone [9,41]. Because T1R3 also mediates amino acid sensing (T1R1/T1R3) [13] and gustducin targets multiple GPCRs, the use of T1R2-KO mice for assessing glucose sensing is necessary to avoid confounding effects. Paradoxically, despite the reduced incretin responses during the IG.GTT, T1R2-KO mice were not glucose intolerant, suggesting a compensatory mechanism that prevents the development of hyperglycemia. Indeed, we found reduced glucose absorption in T1R2-KO mice *in vivo* and in isolated intestinal preparations *ex vivo*. Remarkably, glucose absorption in T1R2-KO intestines was fully restored with the administration of teduglutide, suggesting that GLP-2 is downstream effector of T1R2 signaling. This pathway may also be conserved in humans, as we could recapitulate similar effects in human intestinal explants subjected to pharmacological inhibition (lactisole) of STRs in the Ussing chamber. The inhibitory effects of lactisole, which acts on the T1R3 receptor [28], also suggests that the effects of STRs on glucose absorption involve the canonical T1R2/T1R3 receptor heterodimer.

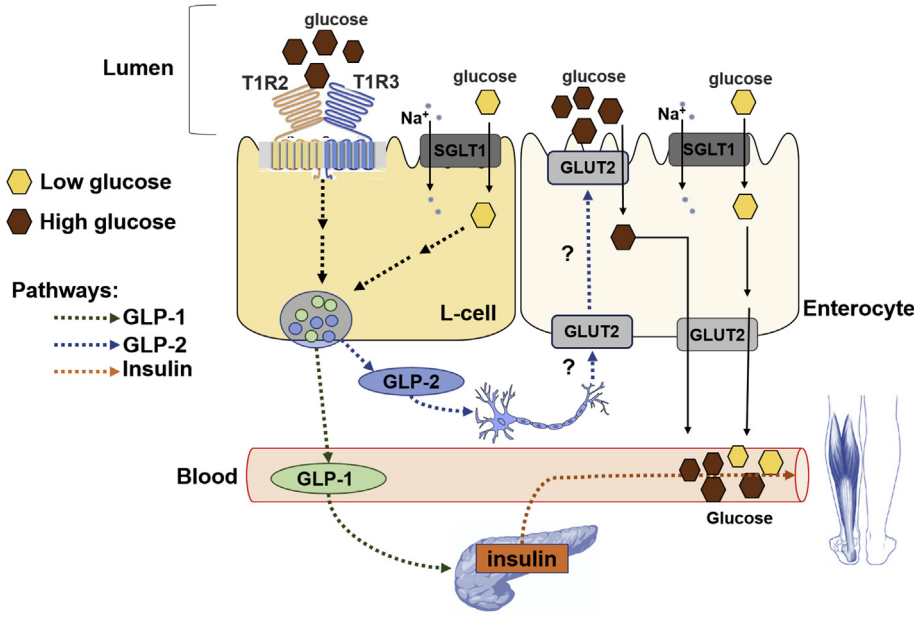

Figure 5: Proposed model for the regulation of post-ingested glucose metabolism by intestinal sweet taste receptor (STR) signaling through the coordinated effects of GLP-1 and GLP-2. At low luminal glucose concentrations such as during a mixed meal, SGLT1-mediated glucose transport in enterocytes is the primary and constitutive pathway for glucose absorption. In L-cells, SGLT1-mediated glucose uptake induces peptide secretion under the same conditions. In contrast, in response to a meal rich in sugars, luminal glucose concentrations rise dramatically, saturating SGLT1 in enterocytes and L-cells. Activation of STRs on L-cells, located primarily at the proximal intestine, potentiates the co-secretion of GLP-1 and GLP-2. Increased GLP-2 in the gut induces paracrine activation of the enteric nervous system which, through yet unknown mechanisms, causes extensive GLUT2 translocation from the basolateral to the apical membrane in enterocytes. This enhances glucose absorption and subsequently increases plasma glucose excursions. The same time, increased GLP-1 in the blood potentiates insulin release by the pancreatic beta-cells which facilitates peripheral glucose disposal, lowering plasma glucose. Thus, STR-mediated GLP-2 and GLP-1 co-secretion acutely coordinates post-ingested glucose homeostasis through complementary mechanisms that promote glucose absorption and disposal, respectively.

Taken together with previously published work on the incretin actions of GLP-1, we suggest that T1R2-mediated co-secretion of GLP-1 and GLP-2 coordinates the fate of postprandial glucose (Figure 5). Accordingly, in response to a glucose-rich meal, GLP-2 potentiates glucose absorption in enterocytes, while proportional co-secretion of GLP-1 potentiates insulin secretion by the beta-cells [42] to counter-balance the increased plasma glucose excursions. Consistent with this hypothesis, elimination of the T1R2 receptor-mediated glucose sensing mechanism tampers both glucose absorption and disposal proportionally, thus maintaining postprandial glucose homeostasis in T1R2-KO mice. Notably, GLP-2 also regulates the transport of luminal amino acids [43] and fatty acids [44], suggesting, along with our findings, an instrumental role of GLP-2 in regulating acute macronutrient absorption which, as shown here, is independent from changes in the intestinal absorptive area or morphology [35].

In addition to elucidating the physiological contribution of intestinal T1R2 receptor in post-ingested glucose regulation, we also found that adaptations in T1R2 glucose-sensing pathway occur in response to dietary nutrient availability. Similar to the downregulation of STRs on beta-cells upon overnight incubation with moderately elevated glucose [22], STRs were promptly downregulated in WT intestines following overnight high-sucrose feeding. This finding may also be applicable to humans because we show that incubation of a human L-cell line at high glucose overnight also reduced STR expression. In agreement, it has been shown that intestinal STR mRNA levels were inversely correlated with fasting glycemia in patients with type 2 diabetes [11] and were also regulated in response to luminal glucose [12]. Similar downregulation was also observed in diet-induced obese and the ob/ob mouse models [45], suggesting that STRs may be under the regulatory control of ambient glucose, luminal or circulating, mediated by yet unknown molecular pathways. The sugar-dependent down-regulation of STRs in WT mice correlated with reduced gut-peptide secretion and glucose absorption *in vivo*, mirroring T1R2-KO mice. Consequently, ablation of T1R2 receptor prevented the development of hyperglycemia after short-term HSD. This is consistent with studies of genetically obese rats that were glucose intolerant but maintained normoglycemia, partially due to reduced intestinal glucose absorption *in vitro* and *in vivo* [46]. Taken together, our findings suggest that reductions in the rate of glucose absorption may be a STR-mediated adaptive response to alleviate exacerbated postprandial hyperglycemia that could rapidly develop, if unrestricted, during high-sugar feeding. However, the precise mechanism for the downregulation of T1R2 expression and the role of intestinal STR signaling in the development of diet-induced metabolic dysregulation requires further investigation, including the use of intestine-specific deletion of T1R2 to uncouple potential peripheral effects of STR function. Finally, it has been shown that STR signaling (i.e. T1R3 and gustducin) is required for the upregulation of SGLT-1 in response to 2-weeks of HSD [39]. In contrast, we didn't observe SGLT-1 upregulation during overnight or 1-week of HSD which may reflect time-dependent effects or other methodological differences, including tissue collection (i.e. mucosal isolation vs. total intestine) that deem further investigation.

Vascular infusion of GLP-2 may regulate GLUT2 translocation [30], while artificial sweeteners may also potentiate GLUT2 translocation in the presence of low glucose in perfused intestines [47]. We found that the T1R2-GLP-2 pathway potentiates glucose absorption specifically through the regulation of GLUT2 transporter and independently of SGLT1 activity. During a regular mixed meal, apical SGLT1 activity is adequate to transport luminal glucose into enterocytes, which then exits through GLUT2 localized in the basolateral membrane (Figure 5).

However, during a meal rich in simple sugars, such as a glucose gavage, GLUT2 translocates to the apical membrane to potentiate glucose uptake [23]. Although SGLT1 is indispensable for intestinal glucose transport [24], the role of GLUT2 has been underestimated because mice with total ablation of the GLUT2 protein maintain normal glucose absorption, likely due to compensatory mechanisms [48]. However, mice with intestine-specific inactivation of GLUT2 show mild reductions in the rate of glucose absorption and excursion at the onset of an oral glucose challenge [49], which parallels the T1R2-KO phenotype in our studies reported here.

The detailed mechanism of GLUT2 activation by GLP-2 remains unclear but is locally modulated and may be partially dependent on enteric nervous system activation. Notably, insulin induces the internalization of GLUT2 [31], so it is plausible that immediate STR activation by ingested glucose promotes rapid GLUT2-dependent glucose absorption through GLP-2. In turn, the co-secretion of GLP-1 stimulates insulin secretion, which, in time, may partially offset the effects of STR signaling on GLUT2. Thus, our studies provide a rationale and a mechanism for the coordinated regulation of glucose metabolism by two gut peptides derived from the same pro-glucagon molecule. The significance of GLUT2 regulation may depend on the magnitude and timing of diverse signals, the spatial and temporal interaction of which requires further investigation. Towards this end, the proximal intestine is likely the primary site of STR stimulation since, at the onset of the gavage (up to 15 min), the glucose solution had transitioned to about half the length of the small intestine in both WT and T1R2-KO mice. Therefore, glucose-dependent stimulation of L-cell subtypes residing at the proximal intestine [40,50] is probably sufficient for triggering a T1R2-GLP-2 paracrine regulatory axis that, through neuronal mechanisms, could activate extensive GLUT2-induced glucose transport throughout the GI tract.

Despite our findings, the role of STRs as glucose sensors has been questioned, first because of the fragmented literature that never provided a cohesive physiological and mechanistic model, and second because artificial sweeteners alone do not stimulate L-cell peptide secretion [51,52]. Instead, it has been proposed that SGLT1 activity on L-cells is the essential sensing mechanism [24,40]. We unequivocally show that the proposed STR-dependent sensory pathway is sensitive to high ambient glucose levels, and it is required to potentiate glucose absorption. Therefore, regular ingestion of artificial sweeteners alone, or low glucose, is likely insufficient to induce physiological responses mediated by STRs. This notion has been supported by others [53,54] and by our own work showing that fructose or saccharin alone cannot stimulate insulin release by the beta-cells, yet potentiated glucose-stimulated insulin secretion dependent on STR activation [21]. Consequently, the presence of two or more glucosensory mechanisms on L-cells is neither redundant nor mutually exclusive and may explain variations in the stimulus-secretion coupling that have been observed in different regions of the intestine [55]. Towards that end, SGTL1 activity on L-cells is essential, yet saturable, providing the basic stimulus for peptide secretion during a normal mixed meal, while receptor-mediated glucosensation becomes crucial during a high sugar meal to enhance GLP-2-dependent apical insertion of GLUT2 in enterocytes. This allows the intestine to maximize glucose absorption over a wider range of dietary glucose levels. The interplay of these sensory machineries has not been directly tested, but it is likely relevant to the metabolic effects of chronic overconsumption of sugars and possible complications from high use of artificial sweeteners.

In conclusion, we demonstrated an integrative pathway for the GLUT2-induced potentiation of glucose absorption during the ingestion of high levels of glucose and showed its dependence on the T1R2 nutrient sensor. Our data also provide a conceptual framework for exploring the physiological significance of GLP-1 and GLP-2 co-secretion in coordinating acute glucose homeostasis. Most notably, we show that this sensory mechanism may be downregulated during metabolic disease progression as an initial adaptive response to excess sugar consumption.

AUTHOR CONTRIBUTIONS

KS and EKA performed experiments, analyzed data, and wrote the manuscript. TEL performed experiments, analyzed data, and edited the manuscript. TH, VV, KK, PV, JPA, and SGD performed experiments. REP and TFO designed research studies, and edited the manuscript. GAK conceived the project, designed research studies, performed experiments, analyzed data, and wrote the manuscript.

ACKNOWLEDGMENTS

This work was supported by the National Institutes of Health (R01DK097757 to TFO and R21DK110489 to GAK) and by institutional funds to GAK. We thank Dr. Edith Brot-Laroche for critical reading of the manuscript; Lorenzo Thomas (SBP) for manuscript preparation and editorial assistance; Dr. Charles Zuker (Columbia University) for mutant mice; Drs. Julio Ayala and Jennifer Ayala (Cardiometabolic Phenotyping Core, SBP) for performing the CLAMS studies; Joshua Smith (Florida Hospital) for human sample collection and processing. Dr. David Terry (Pharmacology Core, SBP) for LC-MS/MS analysis.

CONFLICT OF INTEREST STATEMENT

The authors declare no conflict of interest.

APPENDIX A. SUPPLEMENTARY DATA

Supplementary data related to this article can be found at https://doi.org/10.1016/j.molmet.2018.08.009.

REFERENCES

[1] Furness, J.B., Rivera, L.R., Cho, H.J., Bravo, D.M., Callaghan, B., 2013. The gut as a sensory organ. Nature Reviews Gastroenterology & Hepatology 10: 729–740.

[2] Gribble, F.M., Reimann, F., 2016. Enteroendocrine cells: chemosensors in the intestinal epithelium. Annual Review of Physiology 78:277–299.

[3] Sandoval, D.A., D'Alessio, D.A., 2015. Physiology of proglucagon peptides: role of glucagon and GLP-1 in health and disease. Physiological Reviews 95:513–548.

[4] Lovshin, J.A., Drucker, D.J., 2009. Incretin-based therapies for type 2 diabetes mellitus. Nature Reviews Endocrinology 5:262–269.

[5] Ugleholdt, R., Zhu, X., Deacon, C.F., Orskov, C., Steiner, D.F., Holst, J.J., 2004. Impaired intestinal proglucagon processing in mice lacking prohormone convertase 1. Endocrinology 145:1349–1355.

[6] Janssen, P., Rotondo, A., Mule, F., Tack, J., 2013. Review article: a comparison of glucagon-like peptides 1 and 2. Alimentary Pharmacology & Therapeutics 37:18–36.

[7] Reimann, F., Tolhurst, G., Gribble, F.M., 2012. G-protein-coupled receptors in intestinal chemosensation. Cell Metabolism 15:421–431.

[8] Jang, H.J., Kokrashvili, Z., Theodorakis, M.J., Carlson, O.D., Kim, B.J., Zhou, J., et al., 2007. Gut-expressed gustducin and taste receptors regulate secretion of glucagon-like peptide-1. Proceedings of the National Academy of Sciences of the United States of America 104:15069–15074.

[9] Steinert, R.E., Gerspach, A.C., Gutmann, H., Asarian, L., Drewe, J., Beglinger, C., 2011. The functional involvement of gut-expressed sweet taste receptors in glucose-stimulated secretion of glucagon-like peptide-1 (GLP-1) and peptide YY (PYY). Clinical Nutrition 30:524–532.
[10] Kokrashvili, Z., Mosinger, B., Margolskee, R.F., 2009. T1r3 and alpha-gustducin in gut regulate secretion of glucagon-like peptide-1. Annals of the New York Academy of Sciences 1170:91–94.
[11] Young, R.L., Sutherland, K., Pezos, N., Brierley, S.M., Horowitz, M., Rayner, C.K., et al., 2009. Expression of taste molecules in the upper gastrointestinal tract in humans with and without type 2 diabetes. Gut 58: 337–346.
[12] Young, R.L., Chia, B., Isaacs, N.J., Ma, J., Khoo, J., Wu, T., et al., 2013. Disordered control of intestinal sweet taste receptor expression and glucose absorption in type 2 diabetes. Diabetes 62:3532–3541.
[13] Zhao, G.Q., Zhang, Y., Hoon, M.A., Chandrashekar, J., Erlenbach, I., Ryba, N.J., et al., 2003. The receptors for mammalian sweet and umami taste. Cell 115:255–266.
[14] Ayala, J.E., Bracy, D.P., McGuinness, O.P., Wasserman, D.H., 2006. Considerations in the design of hyperinsulinemic-euglycemic clamps in the conscious mouse. Diabetes 55:390–397.
[15] Heading, R.C., Nimmo, J., Prescott, L.F., Tothill, P., 1973. The dependence of paracetamol absorption on the rate of gastric emptying. British Journal of Pharmacology 47:415–421.
[16] Ayala, J.E., Bracy, D.P., Julien, B.M., Rottman, J.N., Fueger, P.T., Wasserman, D.H., 2007. Chronic treatment with sildenafil improves energy balance and insulin action in high fat-fed conscious mice. Diabetes 56:1025–1033.
[17] Clarke, L.L., 2009. A guide to Ussing chamber studies of mouse intestine. American Journal of Physiology Gastrointestinal and Liver Physiology 296: G1151–G1166.
[18] Moolenbeek, C., Ruitenberg, E.J., 1981. The "Swiss roll": a simple technique for histological studies of the rodent intestine. Laboratory Animals 15:57–59.
[19] Kisielinski, K., Willis, S., Prescher, A., Klosterhalfen, B., Schumpelick, V., 2002. A simple new method to calculate small intestine absorptive surface in the rat. Clinical and Experimental Medicine 2:131–135.
[20] Kenny, A.J., Maroux, S., 1982. Topology of microvillar membrance hydrolases of kidney and intestine. Physiological Reviews 62:91–128.
[21] Kyriazis, G.A., Soundarapandian, M.M., Tyrberg, B., 2012. Sweet taste receptor signaling in beta cells mediates fructose-induced potentiation of glucose-stimulated insulin secretion. Proceedings of the National Academy of Sciences of the United States of America 109:E524–E532.
[22] Kyriazis, G.A., Smith, K.R., Tyrberg, B., Hussain, T., Pratley, R.E., 2014. Sweet taste receptors regulate basal insulin secretion and contribute to compensatory insulin hypersecretion during the development of diabetes in male mice. Endocrinology 155:2112–2121.
[23] Kellett, G.L., Brot-Laroche, E., Mace, O.J., Leturque, A., 2008. Sugar absorption in the intestine: the role of GLUT2. Annual Review of Nutrition 28:35–54.
[24] Gorboulev, V., Schurmann, A., Vallon, V., Kipp, H., Jaschke, A., Klessen, D., et al., 2012. Na(+)-D-glucose cotransporter SGLT1 is pivotal for intestinal glucose absorption and glucose-dependent incretin secretion. Diabetes 61: 187–196.
[25] Duee, P.H., Darcy-Vrillon, B., Blachier, F., Morel, M.T., 1995. Fuel selection in intestinal cells. The Proceedings of the Nutrition Society 54:83–94.
[26] Wu, T., Zhao, B.R., Bound, M.J., Checklin, H.L., Bellon, M., Little, T.J., et al., 2012. Effects of different sweet preloads on incretin hormone secretion, gastric emptying, and postprandial glycemia in healthy humans. The American Journal of Clinical Nutrition 95:78–83.
[27] Karimian Azari, E., Smith, K.R., Yi, F., Osborne, T.F., Bizzotto, R., Mari, A., et al., 2017. Inhibition of sweet chemosensory receptors alters insulin responses during glucose ingestion in healthy adults: a randomized crossover interventional study. The American journal of clinical nutrition 105:1001–1009.
[28] Jiang, P., Cui, M., Zhao, B., Liu, Z., Snyder, L.A., Benard, L.M., et al., 2005. Lactisole interacts with the transmembrane domains of human T1R3 to inhibit sweet taste. Journal of Biological Chemistry 280:15238–15246.
[29] Nauck, M.A., Niedereichholz, U., Ettler, R., Holst, J.J., Orskov, C., Ritzel, R., et al., 1997. Glucagon-like peptide 1 inhibition of gastric emptying outweighs its insulinotropic effects in healthy humans. American Journal of Physiology 273:E981–E988.
[30] Au, A., Gupta, A., Schembri, P., Cheeseman, C.I., 2002. Rapid insertion of GLUT2 into the rat jejunal brush-border membrane promoted by glucagon-like peptide 2. The Biochemical Journal 367:247–254.
[31] Tobin, V., Le Gall, M., Fioramonti, X., Stolarczyk, E., Blazquez, A.G., Klein, C., et al., 2008. Insulin internalizes GLUT2 in the enterocytes of healthy but not insulin-resistant mice. Diabetes 57:555–562.
[32] Shepherd, E.J., Helliwell, P.A., Mace, O.J., Morgan, E.L., Patel, N., Kellett, G.L., 2004. Stress and glucocorticoid inhibit apical GLUT2-trafficking and intestinal glucose absorption in rat small intestine. The Journal of Physiology 560:281–290.
[33] Tee, C.T., Wallis, K., Gabe, S.M., 2011. Emerging treatment options for short bowel syndrome: potential role of teduglutide. Clinical and Experimental Gastroenterology 4:189–196.
[34] Bjerknes, M., Cheng, H., 2001. Modulation of specific intestinal epithelial progenitors by enteric neurons. Proceedings of the National Academy of Sciences of the United States of America 98:12497–12502.
[35] Drucker, D.J., Erlich, P., Asa, S.L., Brubaker, P.L., 1996. Induction of intestinal epithelial proliferation by glucagon-like peptide 2. Proceedings of the National Academy of Sciences of the United States of America 93:7911–7916.
[36] Smith, K.R., Hussain, T., Karimian Azari, E., Steiner, J.L., Ayala, J.E., Pratley, R.E., et al., 2016. Disruption of the sugar sensing receptor T1R2 attenuates metabolic derangements associated with diet-induced obesity. American Journal of Physiology Endocrinology and Metabolism ajpendo 00484 2015.
[37] Smith, K.R., Hussain, T., Karimian Azari, E., Steiner, J.L., Ayala, J.E., Pratley, R.E., et al., 2016. Disruption of the sugar-sensing receptor T1R2 attenuates metabolic derangements associated with diet-induced obesity. American Journal of Physiology Endocrinology and Metabolism 310:E688–E698.
[38] Le, G.M., Tobin, V., Stolarczyk, E., Dalet, V., Leturque, A., Brot-Laroche, E., 2007. Sugar sensing by enterocytes combines polarity, membrane bound detectors and sugar metabolism. Journal of Cellular Physiology 213:834–843.
[39] Margolskee, R.F., Dyer, J., Kokrashvili, Z., Salmon, K.S., Ilegems, E., Daly, K., et al., 2007. T1R3 and gustducin in gut sense sugars to regulate expression of Na+-glucose cotransporter 1. Proceedings of the National Academy of Sciences of the United States of America 104:15075–15080.
[40] Reimann, F., Habib, A.M., Tolhurst, G., Parker, H.E., Rogers, G.J., Gribble, F.M., 2008. Glucose sensing in L cells: a primary cell study. Cell Metabolism 8:532–539.
[41] Gerspach, A.C., Steinert, R.E., Schonenberger, L., Graber-Maier, A., Beglinger, C., 2011. The role of the gut sweet taste receptor in regulating GLP-1, PYY, and CCK release in humans. American Journal of Physiology Endocrinology and Metabolism 301:E317–E325.
[42] Mojsov, S., Weir, G.C., Habener, J.F., 1987. Insulinotropin: glucagon-like peptide I (7-37) co-encoded in the glucagon gene is a potent stimulator of insulin release in the perfused rat pancreas. The Journal of Clinical Investigation 79:616–619.
[43] Lee, J., Koehler, J., Yusta, B., Bahrami, J., Matthews, D., Rafii, M., et al., 2017. Enteroendocrine-derived glucagon-like peptide-2 controls intestinal amino acid transport. Molecular Metabolism 6:245–255.
[44] Hsieh, J., Longuet, C., Maida, A., Bahrami, J., Xu, E., Baker, C.L., et al., 2009. Glucagon-like peptide-2 increases intestinal lipid absorption and chylomicron production via CD36. Gastroenterology 137:997–1005 e1–4.
[45] Herrera Moro Chao, D., Argmann, C., Van Eijk, M., Boot, R.G., Ottenhoff, R., Van Roomen, C., et al., 2016. Impact of obesity on taste receptor expression in extra-oral tissues: emphasis on hypothalamus and brainstem. Scientific Reports 6:29094.

[46] Garcia-Martinez, C., Lopez-Soriano, F.J., Argiles, J.M., 1993. Intestinal glucose absorption is lower in obese than in lean Zucker rats. The Journal of Nutrition 123:1062—1067.

[47] Mace, O.J., Affleck, J., Patel, N., Kellett, G.L., 2007. Sweet taste receptors in rat small intestine stimulate glucose absorption through apical GLUT2. Journal of Physiology 582:379—392.

[48] Stumpel, F., Burcelin, R., Jungermann, K., Thorens, B., 2001. Normal kinetics of intestinal glucose absorption in the absence of GLUT2: evidence for a transport pathway requiring glucose phosphorylation and transfer into the endoplasmic reticulum. Proceedings of the National Academy of Sciences of the United States of America 98:11330—11335.

[49] Schmitt, C.C., Aranias, T., Viel, T., Chateau, D., Le Gall, M., Waligora-Dupriet, A.J., et al., 2017. Intestinal invalidation of the glucose transporter GLUT2 delays tissue distribution of glucose and reveals an unexpected role in gut homeostasis. Molecular Metabolism 6:61—72.

[50] Haber, A.L., Biton, M., Rogel, N., Herbst, R.H., Shekhar, K., Smillie, C., et al., 2017. A single-cell survey of the small intestinal epithelium. Nature 551:333—339.

[51] Bryant, C., McLaughlin, J., 2016. Low calorie sweeteners: evidence remains lacking for effects on human gut function. Physiology & Behavior 164:482—485.

[52] Fujita, Y., Wideman, R.D., Speck, M., Asadi, A., King, D.S., Webber, T.D., et al., 2009. Incretin release from gut is acutely enhanced by sugar but not by sweeteners in vivo. American Journal of Physiology Endocrinology and Metabolism 296:E473—E479.

[53] Brown, R.J., Walter, M., Rother, K.I., 2009. Ingestion of diet soda before a glucose load augments glucagon-like peptide-1 secretion. Diabetes Care 32: 2184—2186.

[54] Pepino, M.Y., Tiemann, C.D., Patterson, B.W., Wice, B.M., Klein, S., 2013. Sucralose affects glycemic and hormonal responses to an oral glucose load. Diabetes Care 36:2530—2535.

[55] Kuhre, R.E., Christiansen, C.B., Saltiel, M.Y., Wewer Albrechtsen, N.J., Holst, J.J., 2017. On the relationship between glucose absorption and glucose-stimulated secretion of GLP-1, neurotensin, and PYY from different intestinal segments in the rat. Physiological Reports 5.

